The Classical and Quantum Hydrodynamic Models

Carl L. Gardner[1]
Department of Computer Science and Department of Mathematics
Duke University
Durham, NC 27706

Abstract

The classical and quantum hydrodynamic equations are presented in a unified formulation and the 3D transport equations are mathematically classified. The 1D steady-state classical and quantum equations are discretized in conservation form using an upwind method. A classical hydrodynamic simulation of a steady-state electron shock wave in a one micron Si semiconductor device at 77 K is presented and compared with a DAMOCLES simulation of the Boltzmann equation. Quantum hydrodynamic simulations of a resonant tunneling diode are presented which show charge buildup in the quantum well and negative differential resistance in the current-voltage curve.

I. Introduction

Electron propagation in a semiconductor crystal is well modeled down to submicron scales by the classical hydrodynamic model. The classical hydrodynamic equations can be extended to include quantum effects by incorporating the first quantum corrections. These $O(\hbar^2)$ terms allow particle tunneling through potential barriers and particle buildup in potential wells.

The aim of this paper is to give a unified presentation of the classical and quantum hydrodynamic conservation laws and of their mathematical classification and numerical discretization. I will also present a classical hydrodynamic (CHD) simulation of an electron shock wave in a one micron Si n^+-n-n^+ device at 77 K and quantum hydrodynamic (QHD) simulations of resonant tunneling in an $GaAs/Al_xGa_{1-x}As$ diode at 77 K.

The classical and quantum hydrodynamic conservation laws have the same form:

$$\frac{\partial n}{\partial t}+\frac{\partial}{\partial x_i}(nu_i)=0 \tag{1}$$

$$\frac{\partial p_j}{\partial t}+\frac{\partial}{\partial x_i}(u_ip_j-P_{ij})=-n\frac{\partial V}{\partial x_j}-\frac{p_j}{\tau_p} \tag{2}$$

$$\frac{\partial W}{\partial t}+\frac{\partial}{\partial x_i}(u_iW-u_jP_{ij}+q_i)=-nu_i\frac{\partial V}{\partial x_i}-\frac{\left(W-\frac{3}{2}nT_0\right)}{\tau_w} \tag{3}$$

[1]Research supported in part by the U.S. Army Research Office under grant DAAL03-91-G-0146 and by the National Science Foundation under grant NSF-DMS-92-04189.

where n is the electron density, $\mathbf{u}$ is the velocity, $\mathbf{p}$ is the momentum density, P_{ij} is the stress tensor, $V = -e\phi$ is the potential energy, ϕ is the electric potential, $e > 0$ is the electronic charge, W is the energy density, $\mathbf{q}$ is the heat flux, and T_0 is the lattice temperature in energy units (k_B is set equal to 1). Indices i, j equal 1, 2, 3, and repeated indices are summed over. Eq. (1) expresses conservation of electron number, Eq. (2) expresses conservation of momentum, and Eq. (3) expresses conservation of energy. The collision terms in Eqs. (2) and (3) are modeled here by the standard relaxation time approximation, with momentum and energy relaxation times τ_p and τ_w.

The classical and quantum hydrodynamic equations can be derived from a moment expansion of the Wigner-Boltzmann equation. The classical equations are obtained by setting $\hbar = 0$. To close the moment expansion at three moments, we have to define e.g. $\mathbf{p}$, P_{ij}, W, and $\mathbf{q}$ in terms of n, $\mathbf{u}$, and T, where T is the electron temperature.

In the simplest approximation, the heat flux is specified by the Fourier law $\mathbf{q} = -\kappa\nabla T$. For the $O(\hbar^2)$ "momentum-shifted" thermal equilibrium Wigner distribution function, the momentum density $\mathbf{p} = mn\mathbf{u}$, where m is the effective electron mass, the stress tensor is given by

$$P_{ij} = -nT\delta_{ij} + \frac{\hbar^2 n}{12m}\frac{\partial^2}{\partial x_i \partial x_j}\log(n) + O(\hbar^4) \tag{4}$$

and the energy density by

$$W = \frac{3}{2}nT + \frac{1}{2}mnu^2 - \frac{\hbar^2 n}{24m}\nabla^2\log(n) + O(\hbar^4)\ . \tag{5}$$

I derived the full three-dimensional quantum hydrodynamic model for the first time by a moment expansion of the Wigner-Boltzmann equation in Ref. [1]. The quantum correction to the energy density was first derived by Wigner [2]. The quantum correction to the stress tensor was proposed by Ancona and Tiersten [3] on general thermodynamical grounds and derived by Ancona and Iafrate [4] in the Wigner formalism. In the one-dimensional case, the 3D QHD equations reduce to the QHD model of Grubin and Kreskovsky [5].

The actual expansion parameter in the QHD equations is $\hbar^2/8mTl^2$, where l is a characteristic length scale of the problem [4]. For the resonant tunneling diode simulations in section V with $T \approx T_0 = 77$ K and $l = 100$ Å, the expansion parameter ≈ 0.23.

The transport equations (1)–(3) are coupled to Poisson's equation for the electric potential energy

$$\nabla\cdot(\epsilon\nabla V) = e^2(N_D - N_A - n) \tag{6}$$

where ϵ is the dielectric constant, N_D is the density of donors, and N_A is the density of acceptors.

II. Classification of the Hydrodynamic Equations

To classify the hydrodynamic equations, rewrite the hydrodynamic equations (1)–(3) and (6) (with $\tau_p,\ \tau_w \to \infty$) in terms of n, $\mathbf{u}$, and T:

$$\frac{\partial n}{\partial t} + \frac{\partial}{\partial x_i}(nu_i) = 0 \tag{7}$$

$$\frac{\partial u_j}{\partial t} + u_i \frac{\partial u_j}{\partial x_i} + \frac{1}{mn}\frac{\partial}{\partial x_j}(nT) - \frac{\hbar^2}{12m^2 n}\frac{\partial}{\partial x_i}\left(n\frac{\partial^2}{\partial x_i \partial x_j}\log(n)\right) + \frac{1}{m}\frac{\partial V}{\partial x_j} = 0 \qquad (8)$$

$$\frac{\partial T}{\partial t} + u_i \frac{\partial T}{\partial x_i} + \frac{2}{3}T\frac{\partial u_i}{\partial x_i} - \frac{2}{3n}\frac{\partial}{\partial x_i}\left(\kappa\frac{\partial T}{\partial x_i}\right) + \frac{\hbar^2}{36mn}\frac{\partial}{\partial x_i}(n\nabla^2 u_i) = 0 \qquad (9)$$

$$-\nabla(\epsilon\nabla V) + e^2(N_D - N_A - n) = 0\ . \qquad (10)$$

Then linearize the PDEs (7)–(10) with respect to a Fourier mode perturbation, and freeze coefficients. Set

$$\begin{bmatrix} n \\ u_i \\ T \\ V \end{bmatrix} = \begin{bmatrix} \overline{n} \\ \overline{u_i} \\ \overline{T} \\ \overline{V} \end{bmatrix} + e^{-\sigma t + i\mathbf{k}\cdot\mathbf{x}} \begin{bmatrix} \delta n \\ \delta u_i \\ \delta T \\ \delta V \end{bmatrix} \qquad (11)$$

where $[\overline{n},\ \overline{u_i},\ \overline{T},\ \overline{V}]$ is a solution of the hydrodynamic equations.

Next write the linearized hydrodynamic equations in terms of the symbol $\mathcal{S}$ of the linearized PDE system (7)–(10) as

$$-\operatorname{diag}\{\sigma,\ \sigma,\ \sigma,\ \sigma,\ \sigma,\ 0\}\,[\delta n,\ \delta u_i,\ \delta T,\ \delta V] + \mathcal{S}\,[\delta n,\ \delta u_i,\ \delta T,\ \delta V] = 0 \qquad (12)$$

As $|\mathbf{k}| \to \infty$, $\mathcal{S} - \operatorname{diag}\{\sigma,\ \sigma\delta_{ij},\ \sigma,\ 0\}$ has the form

$$\begin{array}{c} \\ j \downarrow \end{array} \begin{array}{c} \qquad\qquad i \rightarrow \\ \begin{bmatrix} i\mathbf{k}\cdot\mathbf{u} - \sigma & ik_i n & 0 & 0 \\ ik_j\frac{T}{mn} + ik_j k^2\frac{\hbar^2}{12m^2 n} & (i\mathbf{k}\cdot\mathbf{u} - \sigma)\delta_{ij} & i\frac{k_j}{m} & i\frac{k_j}{m} \\ ik_i\frac{\hbar^2}{36mn}\nabla^2 u_i & \frac{2}{3}ik_i T - ik_i k^2\frac{\hbar^2}{36m} & i\mathbf{k}\cdot\mathbf{u} + \frac{2}{3}k^2\frac{\kappa}{n} - \sigma & 0 \\ 0 & 0 & 0 & k^2\epsilon \end{bmatrix} \end{array} \qquad (13)$$

where i labels columns in the velocity perturbation δu_i and j labels rows in the velocity equation (8). I have dropped the bar over the solution $[n,\ u_i,\ T,\ V]$, and have separately kept the leading terms in k for the limits $\hbar \to 0$ and $\kappa \to 0$.

The mathematical type of the PDE system is determined by the asymptotic eigenvalues σ of the symbol as $|\mathbf{k}| \to \infty$. We need only consider the upper 5×5 block $\mathcal{S}_5$ of the symbol, since the coupling of the transport equations (7)–(9) to Poisson's equation (10) only introduces the elliptic Poisson mode, and does not affect the modes of the transport equations.

There are three physically interesting cases to consider:

(1) $\hbar = 0$, $\kappa = 0$ (electrogasdynamics). The eigenvalues of the symbol $\mathcal{S}_5$ and corresponding modes are

$$\begin{cases} i(\mathbf{k}\cdot\mathbf{u} \pm kc) & \text{hyperbolic} \\ i\mathbf{k}\cdot\mathbf{u} & \text{hyperbolic, multiplicity 3} \end{cases} \qquad (14)$$

where $c = \sqrt{5T/3m}$. There are five nonlinear waves in classical electrogasdynamics corresponding to the five hyperbolic modes: two shock waves and three contact waves. Two

contact waves can be labeled by a jump in the tangential velocity $\mathbf{u}_t$ across the wave, and one contact wave by a jump in the temperature T.

(2) $\hbar = 0$, $\kappa > 0$ (hydrodynamic model or electrogasdynamics with heat conduction). The eigenvalues of the symbol $\mathcal{S}_5$ and corresponding modes are

$$\begin{cases} i(\mathbf{k}\cdot\mathbf{u} \pm kc) & \text{hyperbolic} \\ i\mathbf{k}\cdot\mathbf{u} & \text{hyperbolic, multiplicity 2} \\ \frac{2}{3}k^2\kappa/n + i\mathbf{k}\cdot\mathbf{u} & \text{parabolic} \end{cases} \tag{15}$$

where $c = \sqrt{T/m}$. With heat conduction, there are four nonlinear waves [6] in the CHD model corresponding to the four hyperbolic modes: two shock waves and two contact waves. The two contact waves can be labeled by a jump in the tangential velocity $\mathbf{u}_t$ across the wave. The contact wave corresponding to a discontinuity in T has disappeared due to the parabolic heat conduction term $\nabla\cdot(\kappa\nabla T)$ in Eq. (3).

(3) $\hbar \neq 0$, $\kappa > 0$ (quantum hydrodynamic model). The eigenvalues of the symbol $\mathcal{S}_5$ and corresponding modes are

$$\begin{cases} \pm ik^2\frac{\hbar}{\sqrt{12m}} & \text{Schrödinger} \\ i\mathbf{k}\cdot\mathbf{u} & \text{hyperbolic, multiplicity 2} \\ \frac{2}{3}k^2\kappa/n & \text{parabolic} \end{cases} \tag{16}$$

There are two contact discontinuities (in $\mathbf{u}_t$) in the QHD model corresponding to the two hyperbolic modes. Note that two of the hyperbolic modes (which allow shock discontinuities to form) in the classical hydrodynamic model have become Schrödinger modes when the quantum corrections are included.

Well-posed boundary conditions for the 2D (and by extension 3D) classical hydrodynamic model are formulated in Ref. [7], assuming subsonic flow at the inflow and outflow boundaries. Here I will simply note that in one dimension, the CHD model (with heat conduction) has two hyperbolic modes, one parabolic mode, and one elliptic mode, and the QHD model (with heat conduction) has two Schrödinger modes, one parabolic mode, and one elliptic mode. Thus six boundary conditions are necessary for the CHD model and eight boundary conditions for the QHD model. Well-posed boundary conditions for the 1D CHD equations are $n = N_D$, and $T = T_0$ (or $\partial T/\partial x = 0$) at x_{min} and x_{max}, with a bias ΔV across the device: $V(x_{min}) = T\log(n/n_i)$ and $V(x_{max}) = T\log(n/n_i) + e\Delta V$, where n_i is the intrinsic electron concentration. For the 1D QHD equations, I add $\partial n/\partial x = 0$ at x_{min} and x_{max}.

III. The Second Upwind Method

I will discretize the 1D steady-state hydrodynamic equations using an upwind method adapted from computational fluid dynamics. Since the upwind method requires velocity values $u_{-\frac{1}{2}}$, $u_{\frac{1}{2}}$, $u_{\frac{3}{2}}$, $\cdots$, $u_{N-\frac{1}{2}}$, $u_{N+\frac{1}{2}}$ at the midpoints of the elements l_i $(i = 1, \cdots, N)$

connecting grid points $i-1$ and i, I will use a staggered grid for u. (I impose a computational Neumann boundary condition $du/dx = 0$ at $i = 0$ and $i = N$ to determine $u_{-\frac{1}{2}}$ and $u_{N+\frac{1}{2}}$.) The variables n, T, and V are defined at the grid points $i = 0,\ 1,\ \cdots,\ N-1,\ N$. The boundary conditions specify n, T, and V (and dn/dx for the QHD model) at $i = 0$ and $i = N$.

In one dimension, the steady-state CHD and QHD models consist of the three nonlinear conservation laws for electron number, momentum, and energy, plus Poisson's equation:

$$\begin{bmatrix} f_n \\ f_u \\ f_T \\ f_V \end{bmatrix} = \frac{d}{dx}\begin{bmatrix} ug_n \\ ug_u \\ ug_T \\ 0 \end{bmatrix} + \begin{bmatrix} 0 \\ h_u \\ h_T \\ h_V \end{bmatrix} + \begin{bmatrix} 0 \\ s_u \\ s_T \\ s_V \end{bmatrix} = 0 \tag{17}$$

where (set $\hbar = 0$ for the CHD model)

$$g_n = n \tag{18}$$

$$g_u = mnu \tag{19}$$

$$g_T = \frac{5}{2}nT + \frac{1}{2}mnu^2 - \frac{\hbar^2 n}{8m}\frac{d^2}{dx^2}\log(n) + nV \tag{20}$$

$$h_u = \frac{d}{dx}(nT) - \frac{d}{dx}\left(\frac{\hbar^2 n}{12m}\frac{d^2}{dx^2}\log(n)\right) + n\frac{dV}{dx} \tag{21}$$

$$h_T = -\frac{d}{dx}\left(\kappa\frac{dT}{dx}\right) \tag{22}$$

$$h_V = \epsilon\frac{d^2V}{dx^2} \tag{23}$$

$$s_u = \frac{mnu}{\tau_p} \tag{24}$$

$$s_T = \left(\frac{3}{2}nT + \frac{1}{2}mnu^2 - \frac{\hbar^2 n}{24m}\frac{d^2}{dx^2}\log(n) - \frac{3}{2}nT_0\right)/\tau_w \tag{25}$$

$$s_V = e^2(N_D - N_A - n)\ . \tag{26}$$

Equations $f_n = 0$, $f_T = 0$, and $f_V = 0$ are enforced at the interior grid points $i = 1,\ \cdots,\ N-1$, while equation $f_u = 0$ is enforced at the midpoints of the elements l_i, $i = 1,\ \cdots\ N$.

In the second upwind method, the advection terms $d(ug)/dx$ in Eq. (17) are discretized using second upwind differences[2]

$$\frac{d}{dx}(ug)_i \approx (u_{i+\frac{1}{2}}g_R - u_{i-\frac{1}{2}}g_L)/\Delta x \tag{27}$$

[2]The second upwind method is a conservative extension of the original first-order upwind method.

where

$$g_R = \begin{cases} g_i & (u_{i+\frac{1}{2}} > 0) \\ g_{i+1} & (u_{i+\frac{1}{2}} < 0) \end{cases}, \quad g_L = \begin{cases} g_{i-1} & (u_{i-\frac{1}{2}} > 0) \\ g_i & (u_{i-\frac{1}{2}} < 0) \end{cases} \tag{28}$$

and second-order central differences are used for h_u, h_T, h_V, and s_T.

I use Newton's method to linearize the discretized version of Eq. (17):

$$J \begin{bmatrix} \delta n \\ \delta u \\ \delta T \\ \delta V \end{bmatrix} = - \begin{bmatrix} f_n \\ f_u \\ f_T \\ f_V \end{bmatrix} = -f, \quad \begin{bmatrix} n \\ u \\ T \\ V \end{bmatrix} \leftarrow \begin{bmatrix} n \\ u \\ T \\ V \end{bmatrix} + t \begin{bmatrix} \delta n \\ \delta u \\ \delta T \\ \delta V \end{bmatrix} \tag{29}$$

where J is the Jacobian and t is a damping factor between 0 and 1, chosen to insure that the norm of the residual f decreases monotonically.

IV. CHD Simulation of the Electron Shock Wave

The nonlinear hyperbolic modes of the CHD model allow shock waves to develop. A steady-state electron shock wave in a semiconductor device was first simulated in Ref. [8]. The shock simulation has been confirmed by a Monte Carlo simulation of Laux of the Boltzmann equation using the DAMOCLES [9] program. The semiconductor device is an $n^+ - n - n^+$ Si diode at 77 K with 0.1 micron source and drain, with n^+ doping density $N_D = 10^{18}$ cm^{-3}, and a 1.0 micron channel, with n doping density $N_D = 10^{15}$ cm^{-3}.

For the momentum and energy relaxation times in the hydrodynamic model, I use modified Baccarani-Wordemann models:

$$\tau_p = \tau_{p0} \frac{T_0}{T} \tag{30}$$

$$\tau_w = \frac{\tau_p}{2} \left(1 + \frac{\frac{3}{2}T}{\frac{1}{2}mv_s^2} \right) \tag{31}$$

where the low-energy momentum relaxation time τ_{p0} is set equal to 1.67 picoseconds from the DAMOCLES data for 0.00995 eV electrons in homogeneous Si and $v_s = v_s(T_0)$ is the saturation velocity. For Si at 77 K, $m = 0.24\ m_e$ and $v_s = 1.2 \times 10^7$ cm/s.

The hydrodynamic and Boltzmann simulations agree remarkedly well [10] when the amount of heat conduction in the hydrodynamic model is adjusted. The best fit for the thermal conductivity κ in the Wiedemann-Franz law for heat conduction

$$\mathbf{q} = -\kappa \nabla T, \quad \kappa = \kappa_0 \tau_{p0} n T_0 / m, \tag{32}$$

is given by $\kappa_0 = 0.05$.

Figs. 1 and 2 compare the hydrodynamic and DAMOCLES simulations of the 77 K electron shock wave in Si at a bias $\Delta V = 1$ volt. DAMOCLES calculates a current of 4500 amps/cm^2, very close to the hydrodynamic value of 4460 amps/cm^2. The velocity plot Fig. 1 most clearly shows the shock profile, which is spread out slightly due to the parabolic heat conduction term in the CHD model. The flow is supersonic at the velocity

peak just inside the channel, and subsonic at the end of the "velocity overshoot" wave where the velocity makes a "bend" to a constant value in the channel.

The DAMOCLES velocity exhibits a Mach 2.1 shock profile based on both internal evidence[3] and comparison with the hydrodynamic simulation.

The type of velocity overshoot illustrated in Fig. 1 is always associated with a shock wave for the $n^+ - n - n^+$ diode. As the electrons enter the channel, the electron velocity increases rapidly to a peak value greater than the saturation velocity v_s. At the same time, the electron temperature falls slightly as the electrons overcome the small potential barrier at the source/channel junction. Thus the electron Mach number M near the velocity peak is greater than $v_s/c > v_s/c_0$, where $c = \sqrt{T/m}$ is the soundspeed at temperature T and c_0 is the soundspeed at the ambient temperature T_0. For Si at 77 K, $v_s = 1.2 \times 10^7$ cm/s, $c_0 = 7.0 \times 10^6$ cm/s, and $M > 1.7$. On the other hand, the electron flow near the channel/drain is subsonic since $v \approx v_s$, while $T \gg T_0$, making $c \gg v_s$.

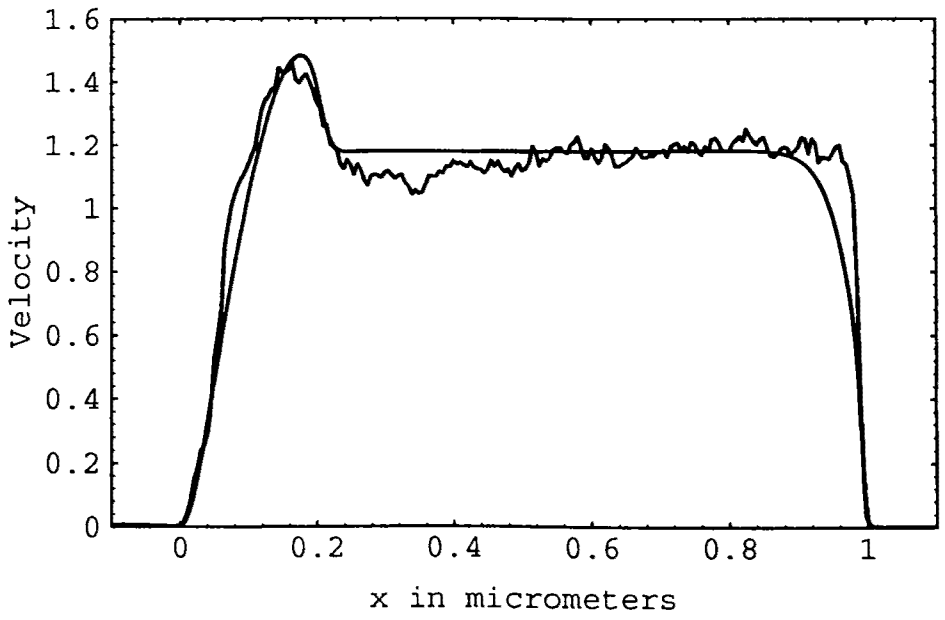

Figure 1: Hydrodynamic and Monte Carlo electron velocity in 10^7 cm/s for $\Delta V = 1$ volt. The jagged curve is the DAMOCLES result. The channel is between $x = 0$ and $x = 1$ micron.

The transition from supersonic flow to subsonic flow in general necessitates a shock wave in gas dynamics[4]—that is, a wave over which density, velocity, and (if heat conduction equals zero) temperature change very rapidly. The n^+ drain in the source–channel–

[3]The electron temperature $T \approx 77$ K at the shock wave. Using the effective electron mass approximation, the electron Mach number $M = v/c = v/\sqrt{T/m} \approx 2.1$.

[4]See Courant and Friedrichs [11], pp. 380–387.

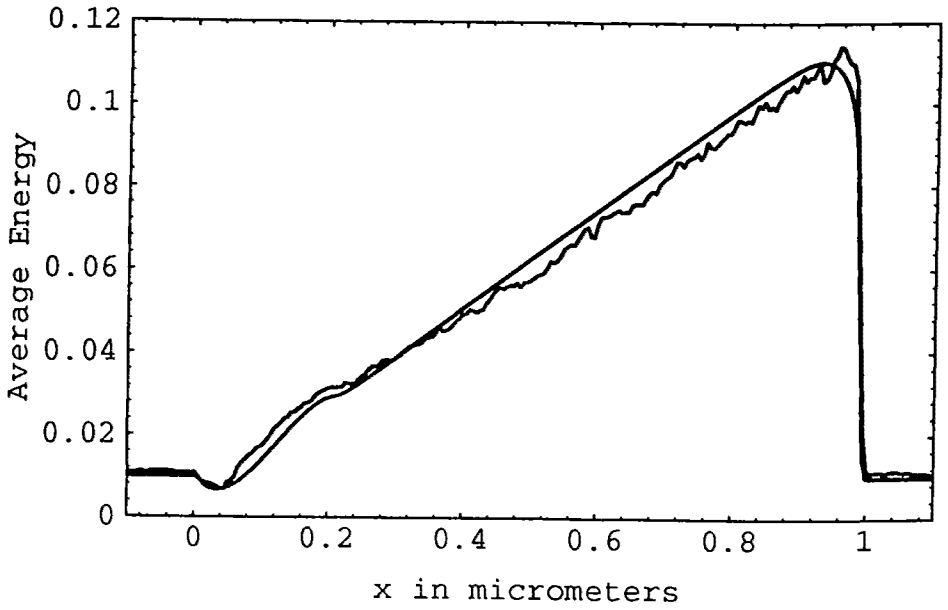

Figure 2: Hydrodynamic and Monte Carlo electron average energy in eV for $\Delta V = 1$ volt. The jagged curve is the DAMOCLES result.

drain structure of the diode provides the mechanism that forces a supersonic flow in the channel back down to subsonic flow.

The excellent agreement between the hydrodynamic and DAMOCLES results is remarkable in that the hydrodynamic model is orders of magnitude faster than Monte Carlo simulation of the Boltzmann equation. The hydrodynamic model also provides a mathematical framework in which to understand the velocity overshoot wave in the $n^+ - n - n^+$ diode.

V. QHD Simulation of the Resonant Tunneling Diode

The behavior of quantum devices that depend on particle tunneling through potential barriers and/or charge buildup in potential wells can be efficiently simulated using the QHD model. Here I will present simulations of a GaAs resonant tunneling diode with double $Al_xGa_{1-x}As$ barriers, with barrier height $\mathcal{B} = 0.209$ eV. The diode consists of an n^+ source (at the left) and an n^+ drain (at the right) with the doping density $N_D = 10^{18}$ cm^{-3}, and an n channel with $N_D = 5 \times 10^{15}$ cm^{-3} (see Fig. 3). The channel is 250 Å long, the barriers are 50 Å wide, and the quantum well between the barriers is 50 Å wide. To enhance resonant tunneling, the device has 50 Å spacers between the barriers and the contacts.

The barrier height $\mathcal{B}$ is incorporated into the QHD transport equations (1)–(3) by replacing $V \to V + \mathcal{B}$. (Poisson's equation is not changed.)

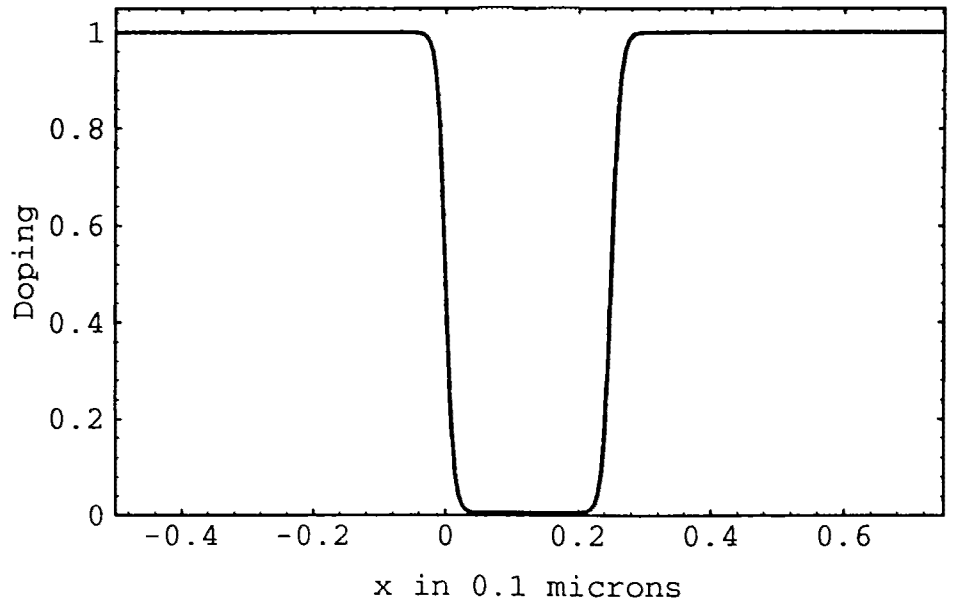

Figure 3: Doping/10^{18} cm^{-3}.

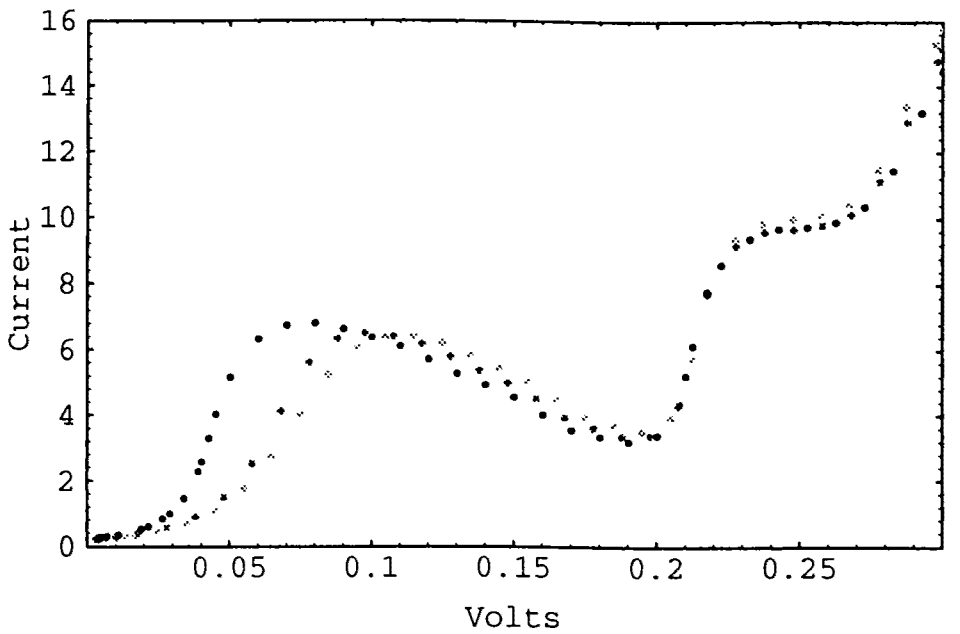

Figure 4: Current density in kiloamps/cm^2 vs. voltage for the resonant tunneling diode at 77 K. $\kappa_0 = 0.2$ (black), 0.4 (dark gray), and 0.6 (gray). The dots represent computed solution points.

For lower valley electrons in GaAs at 77 K, the low-energy momentum relaxation time τ_{p0} in Eqs. (30) and (31) is set equal to 0.9 picoseconds, the effective electron mass $m = 0.063\ m_e$, and the saturation velocity (in Eq. (31)) $v_s \approx 2 \times 10^7$ cm/s. The dielectric constant $\epsilon = 12.9$ for GaAs.

Current-voltage curves for the resonant tunneling diode at 77 K are plotted in Fig. 4 for three different values of κ_0 in the expression for thermal conductivity (32). These are the first simulations [1] of the full QHD equations to show NDR in the resonant tunneling diode.

The peak of the current-voltage curve occurs as the electrons tunneling through the first barrier come into resonance with the the ground state of the quantum well. Note the presence of a "shoulder" in the current-voltage curve around $\Delta V = 0.25$ volts. The shoulder signals the location of the first virtual state of the quantum well. The location of the valley and shoulder can be qualitatively understood from the energy levels of a square well. For a 50 Å wide 0.209 eV high GaAs finite square well, there is just one bound state energy level at 0.079 eV. The energy of the first virtual state of the well is 0.24 eV.

The main effect of larger values of κ_0 is to shift the peak of the current-voltage curve to the right. With lower values of κ_0, the electrons have a higher average energy as they impinge upon the first barrier, and therefore resonate with the well at a lower applied voltage.

A physically relevant value of κ_0 is approximately 0.4 for this device. The peak to valley current ratio of 1.95 agrees quantitatively with experimental ratios for similar devices.

Fig. 5 shows the dramatic charge enhancement in the quantum well typical of the resonant tunneling diode for applied voltages of $\Delta V = 0.097$ (peak), 0.191 (valley), and 0.22 volts (just before the shoulder) (with $\kappa_0 = 0.4$). The electron density at the center of the quantum well increases as ΔV increases, and is more than two orders of magnitude larger than the background doping density. Note the depletion of electrons around the channel-drain junction.

As illustrated in Fig. 6, the electrons spend the longest time in the quantum well for voltages near ΔV_{valley}. The "dwell" time spent by electrons in the well increases monotonically up to voltages near ΔV_{valley}, and then decreases rapidly. The macroscopic QHD dwell time differs qualitatively from dwell times based on microscopic quantum calculations, which predict that the dwell time is maximum at resonance.

Since the QHD equations have the same form as the classical fluid dynamical equations, well-understood classical boundary conditions can be applied in simulating quantum devices. Moreover, the QHD equations are expressed in terms of the fluid dynamical quantities density, velocity, and temperature. These classical fluid dynamical concepts enable us to interpret electron behavior in quantum devices in a physically intuitive way. We can define the time spent by an electron in the quantum well or the electron temperature throughout the device in a precise manner. In turn, the intuitive understanding developed through the QHD model sheds light on more fully quantum mechanical descriptions of electron behavior in quantum devices.

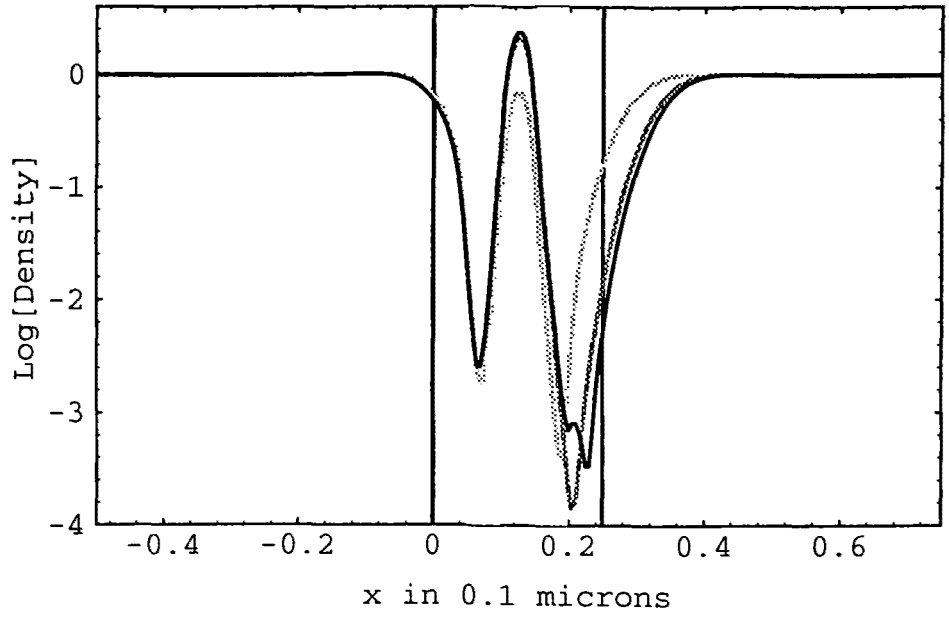

Figure 5: Log[Density/10^{18} cm^{-3}]. The curves are for $\Delta V = 0.097$ (gray), 0.191 (dark gray), and 0.22 (black) volts.

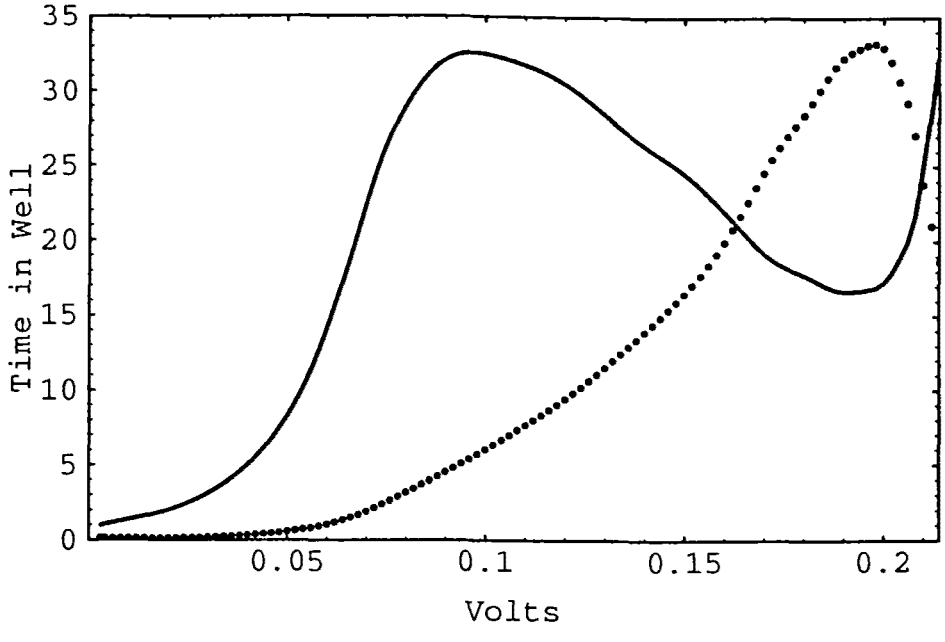

Figure 6: Time in picoseconds (dots) spent by electrons in the quantum well vs. voltage. For reference, a scaled version of the current density (solid line) is also shown.

References

[1] C. L. Gardner, "The quantum hydrodynamic model for semiconductor devices," *SIAM Journal on Applied Mathematics*, to appear, 1993.

[2] E. Wigner, "On the quantum correction for thermodynamic equilibrium," *Physical Review*, vol. 40, pp. 749–759, 1932.

[3] M. G. Ancona and H. F. Tiersten, "Macroscopic physics of the silicon inversion layer," *Physical Review*, vol. B 35, pp. 7959–7965, 1987.

[4] M. G. Ancona and G. J. Iafrate, "Quantum correction to the equation of state of an electron gas in a semiconductor," *Physical Review*, vol. B 39, pp. 9536–9540, 1989.

[5] H. L. Grubin and J. P. Kreskovsky, "Quantum moment balance equations and resonant tunnelling structures," *Solid-State Electronics*, vol. 32, pp. 1071–1075, 1989.

[6] C. L. Gardner, J. W. Jerome, and D. J. Rose, "Numerical methods for the hydrodynamic device model: Subsonic flow," *IEEE Transactions on Computer-Aided Design of Integrated Circuits and Systems*, vol. 8, pp. 501–507, 1989.

[7] F. Odeh and E. Thomann, "On the well-posedness of the two-dimensional hydrodynamic model for semiconductor devices," *COMPEL*, vol. 9, pp. 45–47, 1990.

[8] C. L. Gardner, "Numerical simulation of a steady-state electron shock wave in a submicrometer semiconductor device," *IEEE Transactions on Electron Devices*, vol. 38, pp. 392–398, 1991.

[9] M. V. Fischetti and S. E. Laux, "Monte Carlo analysis of electron transport in small semiconductor devices including band-structure and space-charge effects," *Physical Review*, vol. B 38, pp. 9721–9745, 1988.

[10] C. L. Gardner, "Hydrodynamic and Monte Carlo simulation of an electron shock wave in a one micrometer $n^+ - n - n^+$ diode," *IEEE Transactions on Electron Devices*, vol. 40, pp. 455–457, 1993.

[11] R. Courant and K. O. Friedrichs, *Supersonic Flow and Shock Waves.* New York: Springer-Verlag, 1948.